Journal of Magnetism and Magnetic Materials 468 (2018) 200–208

Contents lists available at ScienceDirect

Journal of Magnetism and Magnetic Materials

journal homepage: www.elsevier.com/locate/jmmm

Research articles

Tunable one-dimensional assembly of magnetic nanoparticles using oscillating magnetic fields at low frequencies for polymer nanocomposite fabrication

Mychal P. Spencer*, David Gao, Namiko Yamamoto

Department of Aerospace Engineering, the Pennsylvania State University, University Park, PA 16802, United States

ARTICLE INFO

Keywords:
Magnetic assembly
Oscillating field
Iron oxide
Nanoparticles
Nanocomposites
Polymer-matrix composites

ABSTRACT

Tunable, one-dimensional (1D) nanofiller assembly using oscillating magnetic fields in the low frequency range (< 5 Hz) is studied as a scalable and energy-efficient method to structure nanofillers within viscous matrices to deliver anisotropic, multi-functional polymer nanocomposites (PNCs). In this work 1D assembly tailoring was first experimentally studied and demonstrated using the model system of superparamagnetic iron oxide nanoparticles (SPIONs, 15 nm, 0.02–0.08 vol%) in DI water using varying magnetic fields (0–5 Hz frequency, 10–100 G magnetic flux density, and square and sinusoidal waveforms). In addition to lateral assembly of nanofillers, when the field oscillation is turned on, transverse assembly can be introduced as the magnetic moments of the particles respond to the changing fields by Brownian rotation. The degree of transverse assembly, in balance with lateral assembly and the resulting nanofiller patterns, was observed to be determined by the magnetic field parameters, magnetic responsiveness of the nanofillers, and the matrix viscosity. Based on this assembly study, PNCs consisting of ferrimagnetic iron oxide nanofillers in a thermoset polymer, with two different linear nanoparticle patterning, were successfully fabricated using small magnetic fields (< 100 G) even in a viscous matrix (70 cP) with a short assembly time of 30 min. This work can contribute to scalable manufacturing and thus bulk application of multi-functional PNCs enabled by more precise nanofiller and interface structuring.

1. Introduction

Bulk application of polymer nanocomposites (PNCs), consisting of nanofillers (carbon, ceramic, metal, etc.) and polymers (thermoset, elastomer, etc.), have been desired for their high mass-specific multi-functional properties (mechanical [1–9], thermal [10], electrical [3,7–9,11,12], magnetic [13,14], and smart [12,15,16]), but has not been achieved due to unknown multi-scale structure-property relationships and missing scalable fabrication. PNCs often exhibit smaller property improvement than theoretical prediction when characterized in macro scale, even with organized implementation of nanofillers [17–20]. While driven by the advanced properties and structuring of nanofillers [8,9,12], PNC properties are critically affected by their boundary conditions (between nanofiller and between nanofillers and polymers) [7,21] as nanofillers alter polymer chains' static and dynamic behaviors and the boundary surface area per volume is large. Such boundary effects on PNC properties are different for each property; for example, with implementation of carbon nanotubes, mechanical toughness increased by mitigating crack-growth due with nanofiller-polymer debonding, void growth, and crack deflection [8,9], while thermal transport property improvement is minimum due to high thermal boundary resistance (Kapitza resistances) [19]. Thus, precise and tunable tailoring of nanofiller structures, including their boundary conditions (inter-nanofiller contacts and nanofiller-polymer bonding), is critical to study these scaling effects per property and to achieve the PNC properties close to the theoretical predictions, but is currently missing.

Nanofiller assembly using oscillating magnetic fields at low frequencies is potentially a solution to the scalable manufacturing of PNCs with tailored nanostructures and nanofiller contacts. While nanofiller integration by deposition on micro-components (such as fibers and cloths [22–24]) is currently a popular method, active nanofiller assembly using external fields has the balanced benefits of scalability and precise structuring of the nanofiller. Nanofiller assembly has been attempted using magnetic fields [20], electric fields [25,26], acoustic fields [27], and even strain deformation [28]. Among these field

* Corresponding author at: 229 Hammond Building, University Park, PA 16802, United States.
E-mail address: mps297@psu.edu (M.P. Spencer).

https://doi.org/10.1016/j.jmmm.2018.08.006
Received 15 April 2018; Received in revised form 6 July 2018; Accepted 4 August 2018
Available online 06 August 2018
0304-8853/

options, the focus of this work is on magnetic assembly due to their non-contact, energy-efficient, fast assembly and patterning capabilities [20,29]. In addition, magnetic assembly does not have limitations set by the dielectric breakdown or electrode polarization using electric fields [3] or by set-up complexity using acoustic fields [27] or strain fields [28]. The nanofiller surfaces can be treated to enhance their dispersion and suspension, and to tune the bonding conditions between nanofillers and polymers [30].

In the past, assembly of microfillers (sphere [31], rods [20], platelets [20,32], etc.) in polymers has been demonstrated using rotating magnetic fields with low flux density (10 G) in a short time (1 h) to fabricate sizable PNCs (50 mm long) [20] with tunable microstructures and mechanical properties [29,32,33]. The magnetic assembly of nanofiller in low viscosity matrices has also been investigated. Both experimental and analytical studies exist about magnetic nanofiller assembly using static or rotating magnetic fields [34–37]. In addition, nanofiller tailoring capability using pulsed fields has been experimentally demonstrated in water; a model system of colloidal suspensions of superparamagnetic latex nanoparticles were assembled through the balancing between particle thermal diffusion and attractive magnetic dipole-dipole interactions [38]. While the effects of gravity decreases due to the nano size, the hydrodynamic forces are size-dependent, and often prevent nanofiller movement especially within viscous polymers [12]. Due to this, thermal diffusion of nanofillers in a polymer matrix is limited, leading to pulsed waveforms being a poor choice for this matrix type. Thus, oscillating magnetic fields, especially of the low frequency range (< 1 Hz), are a novel method to assemble and tailor nanofillers and their interfaces in polymer matrices where transverse particle assembly can be enhanced due to field switching.

In this work, experimental studies were first conducted to understand the effect of the magnetic field (frequency, flux density, and waveform) and nanofiller volume fraction on assembly, including nanofiller contacts, using oscillating magnetic fields. The model system of superparamagnetic iron oxide nanoparticles (SPIONs) dispersed in deionized (DI) water was selected for this parametric study so that magnetic remanence and hydrodynamic drag are minimum. Second, ferrimagnetic nanoparticles were assembled and tailored within DI water and in a polymer matrix. Based on the above assembly studies about the SPIONS, the assembly trends were studied and the capability to tailor nanofillers and their contact conditions within viscous matrices was preliminary demonstrated. Findings from this work will contribute to the development and bulk application of tailored PNCs with advanced, multi-functional properties by enabling scalable manufacturing of PNCs with more precise control of nanofiller structures and their interfaces. The nanofiller volume fractions are kept low (< 0.1%) in this work for easier observation of magnetic assembly and inter-nanofiller distances; relevance of this study to other material systems and to resulting PNC performances will be discussed later.

2. Material and methods

2.1. Magnetic assembly study with SPIONs in DI water

The magnetic assembly behavior of the SPIONs with a low-frequency oscillating magnetic field was captured in real-time and analyzed (see Fig. 1a and b). The SPIONs (Sigma-Aldrich, I7643, 15 nm) are amine-terminated and suspended in an aqueous suspension (50 mg per ml in 1 mM EDTA, pH 7.0), but aggregate (1–5 μm) due to van der Waals forces, electrostatic potential, and/or chemical interactions (see Fig. 1c). The SPION aqueous solutions were prepared to have low volume fractions (0.02–0.08 vol%) to enable observation. SPION aggregates larger than 150 nm will settle [39], and thus the local, as observed, SPION volume fractions were calculated to be higher (approximately 7.5–11.7 vol%) based on processing of the captured images. Superparamagnetism of the SPIONs was confirmed through the anhysteretic magnetic response measured using a vibrating sample magnetometer (MicroSense, ±1200 kA/m) as shown in Fig. 1d. The measured magnetic saturation of 20.6 emu/g and maximum susceptibility of 0.61 are comparable with the values of iron oxide nanoparticles in the literature [40,41].

The magnetic assembly of the SPION aggregates is achieved and captured in real-time using the set-up illustrated in Fig. 1e. In this paper, aggregates refer to the initial SPION groupings as shown in Fig. 1a, and assembly refers to the assembled line features after the field application as shown in Fig. 1b. The SPION aqueous solutions were ultrasonicated (35 kHz) for 5 min, encapsulated in a KOVA Glasstic slide (6 mm × 6 mm area, 0.1 mm height), and mounted between a solenoid pair. Images of SPION assembly were captured using a digital optical microscope (Olympus BX51WI) before and after 15 min of magnetic field application; assembly did not noticeably change beyond 15 min [38]. The solenoid pair (570 turns, 14.8 cm length, 6.51 cm inner diameter, 16-gauge enameled wire, 410 stainless steel core) were connected in series, and driven by a bipolar power supply (Kepco BOP 20–10 M, ± 20 V, ± 10 A) and a function generator (BK Precision, 4014B). The applied magnetic field was varied about the frequency (static, and up to 5.0 Hz), waveform (50% duty cycle square and sinusoidal) and magnetic flux density (peak of ± 10 G, ± 50 G, and ± 100 G for square waves, and RMS peak of ± 14.1 G, ± 70.7 G, and ± 141.4 G for sinusoidal waves). Symmetric square or sinusoidal waveforms were selected, instead of the previously tested pulsed fields [38], to reinforce controlled assembly by switching of the external field direction, rather than by thermal diffusion. The frequency range was kept below 5 Hz to fully enable SPION magnetic moment rotation for the Brownian reorientation mechanism [31]. The minimum flux density was set as 10 G based on the previous related work [20]. The spatial distribution of the magnetic flux density was monitored using a gaussmeter (LakeShore Model 425), and the flux density gradient across the sample was kept below 5% to minimize SPION migration towards the magnetic poles. The captured optical microscope images were processed using Matlab to quantitatively evaluate assembly morphology (see Fig. 1f): the length and width of each assembly, and the separation between the assemblies. The processing details can be found elsewhere [42]. One sample was prepared for each assembly condition, and the characteristic dimensions of the assemblies were averaged over ~100–1000 assemblies for each sample/condition.

3. Theory

Assembly of SPION aggregates using oscillating magnetic fields is governed by forces produced by the external magnetic field, inter-particle magnetic forces, hydrodynamic drag, thermal energy, van der Waals forces, and electrostatic forces. Among these forces, van der Waals and electrostatic forces are assumed to be negligible due to their non-directionality. The forces produced by the external magnetic field are also ignored in this work because only uniform external magnetic fields, while time-varying, were applied to the SPION aggregates. The SPION aggregates are collections of small single-domain (SD) SPIONs, or homogeneous magnetic dipoles [43], and thus have no magnetic remanence due to random reorientations of the SPIONs magnetic moments. The inter-particle magnetic forces due to the locally induced, non-uniform magnetic fields of the aggregates, or the magnetization (M), are expected to largely contribute to assembly of the SPION aggregates [44–46].

3.1. SPION assembly behaviors in magnetic fields

As illustrated in Fig. 2, upon application of a magnetic field, magnetic moments of the SPIONs align along the field direction. When the distance between neighboring spherical aggregates is smaller than the capture radius of $r_c = 2a\lambda^{1/3}$(m), the magnetic attraction overcomes thermal diffusion, and the aggregates form needle-like, elongated assemblies along the field direction (*lateral* assembly) due to the locally

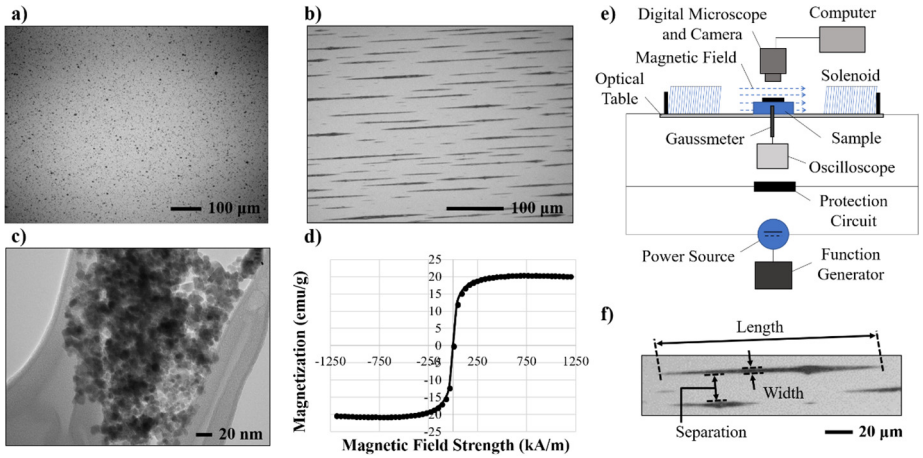

Fig. 1. Magnetic assembly of SPIONs: a) optical microscope image of a SPION aqueous solution (0.08 vol%), b) optical microscope image of SPION assemblies (0.06 vol%) after magnetic field application (± 50 G, 1.0 Hz, 15 min), c) TEM image of a SPION aggregate, d) H-M plot of a SPION aqueous solution (0.08 vol%), e) schematic of the magnetic assembly set-up, and f) the characteristic dimensions of SPION assemblies.

induced fields [47]. a is the aggregate radius (1 μm for the SPIONs) and λ is the dimensionless parameter relating magnetic and thermal effects on spherical aggregates: $\lambda = \pi\mu_0 a^3\chi^2 H^2/9k_BT$ where μ_o is the permeability of free space ($4\pi \times 10^{-7}$ N/A^2), χ is the magnetic susceptibility of the aggregate (0.61 for the SPIONs), H is the magnetic field strength (A/m), k_B is Boltzmann's constant (1.381×10^{-23} J/K), and T is the temperature (298 K for room temperature) [38]. Thus, for the SPION aggregates in DI water (0.04 vol%) to assemble, the capture radius needs to be larger than their average inter-particle distance of 7 μm and therefore requires the magnetic field to be greater than 13 G (13×10^3/

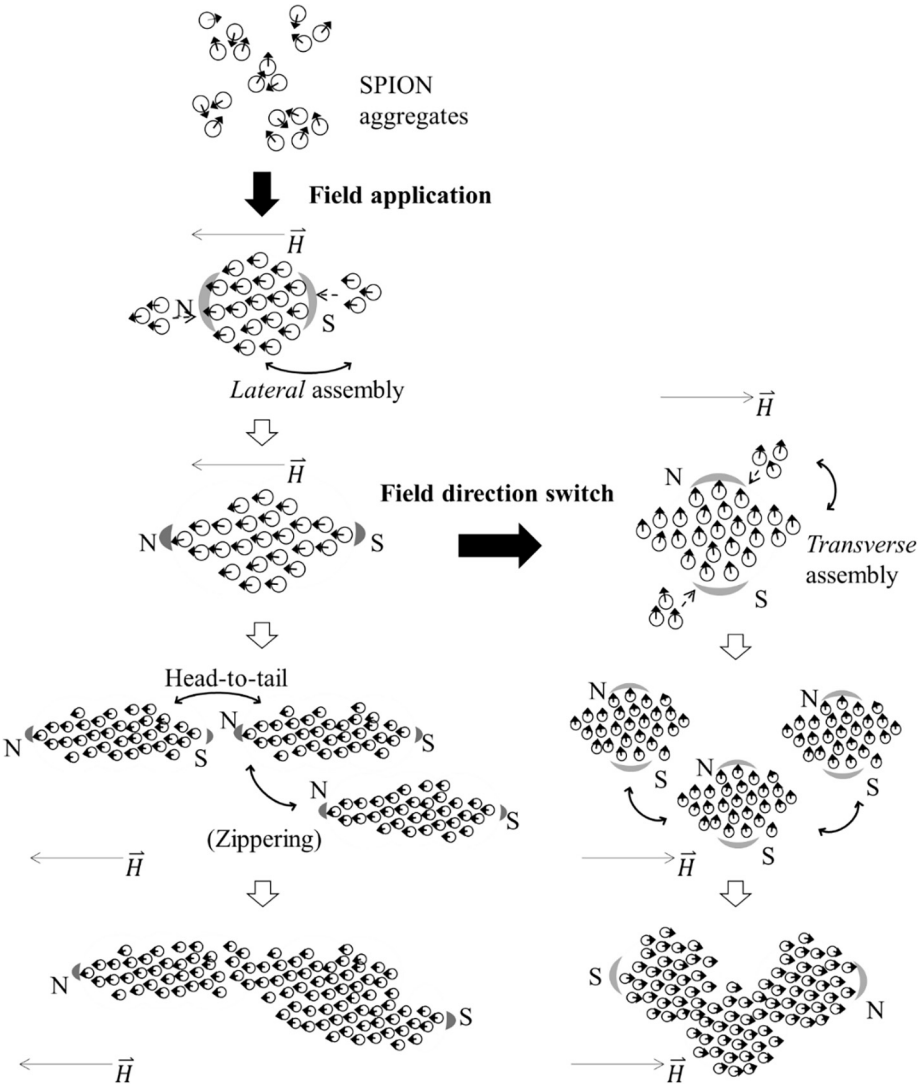

Fig. 2. Schematics of SPION assembly behaviors as a magnetic field is applied and as the field direction is switched. Not to be scaled; more particles exist within the aggregates and assemblies.

4π A/m). The assembly size grows when stronger magnetic fields are applied or with particles of higher susceptibility. As the assemblies become larger and more anisotropic in shape, the locally induced field at the assembly tips becomes stronger promoting additional assembly. Once the assemblies become large enough, neighboring assemblies exhibit head-to-tail attraction to make longer assemblies, or occasionally zippering to produce wider (and longer) assemblies [48]. Similar assembly behaviors have been observed with colloidal suspensions [38]. The assembly size grows until free aggregates and assemblies are depleted within the capture radius of the larger assemblies.

As also illustrated in Fig. 2, upon switching the applied field direction, the SPIONs reorient their magnetic moments along the new field direction [49,50]. In this assembly study, Brownian relaxation (physical particle rotation) occurs faster than Néel relaxation (magnetic domain redefinition) assuming linear response theories [51]; the SPION magnetization varies linearly with the external field ($M_s \ |\vec{B}| \ V < k_B T$, where M_s is the saturation magnetization and V is the SPION magnetic core volume). The Brownian relaxation time at room temperature is calculated as 3.4×10^{-6} s using $\tau_B = \frac{3\eta V_H}{k_B T}$ where η is the matrix viscosity (0.89 cP for water), and V_h is the hydrodynamic volume of a spherical particle (15 nm physical diameter and 21.4 nm hydrodynamic diameter for the SPIONs [52]). The Néel relaxation time at room temperature is calculated as 1.3×10^{-5} s using $\tau_N = \tau_0 e^{KV/k_B T}$ where K is the effective anisotropic energy density (13500 J/m^3 [53]), and τ_0 is the Larmor frequency (estimated as $4.64 \times 10^{-20}/\sqrt{V}$ s or 3.5×10^{-8} s [54]). Thus, with Brownian relaxation being dominant, the SPIONs, if unconstrained, will physically rotate with changes to the applied magnetic field, and will produce a large, albeit temporary, local field gradient in the transverse direction; *transverse* assembly is promoted to form wider (and longer) assemblies.

The combination of the lateral and transverse assembly will contribute to the tailorability of nanoparticle assembly. Transverse assembly can be introduced by the field oscillation as long as the magnetic moments of the SPIONs have sufficient time to respond to the field oscillation and the SPIONs can complete rotation and assemble.

3.2. Transverse assembly behaviors of SPIONs

As noted above, for effective transverse assembly using oscillating magnetic fields, the SPIONs need to reorient their magnetic moments with the changing field's orientation fast enough to complete SPION rotation and assembly. In other words, transverse assembly will not be effective if the field switching occurs too frequently (high frequency). Conversely, magnetic moment rotation will occur faster with larger magnetic fields, with less gradual field transition (square over sinusoidal), or with smaller-sized particles of larger susceptibility, which should promote lateral assembly. The time that a spherical SPION requires to complete their rotation when the magnetic field orientation is switched by 180°can be modeled using Stokes' drag [55]: $2/5mr^2\ddot{\theta} + 8\pi r^3\eta\dot{\theta} + \mu B sin\theta = 0$ where θ is the angle difference between the SPION's magnetic moment and the applied field, m is the mass (9.3×10^{-21} kg for the SPIONs), r is the particle radius (7.5 nm for the SPIONs), η is the matrix viscosity (cP), B is the external magnetic flux density, and an original angle offset of 10^{-5} rad is used. In Fig. 3, how a model SPION magnetic moment rotates to the external field (θ: $\pi \rightarrow 0$)over time is plotted with relevant varying external field parameters (flux density and waveform) and matrix viscosity. As expected, the time for the SPIONs to complete rotation is longer with external fields of small strength and with a sinusoidal waveform, and in more viscous matrices (see Fig. 3a). Such conditions should help promote transverse assembly. Meanwhile, as illustrated in Fig. 3b, as the frequency increases, the SPION magnetic moment cannot catch up with the external field changes and thus may not rotate which will limit transverse assembly. Therefore, to ensure complete rotation of the SPION magnetic moments, and to promote transverse assembly, in addition to lateral assembly, magnetic field oscillation with low frequency ($< \sim 10$ Hz) need to be applied to tailor SPION assembly in viscous polymer matrices.

4. Results and discussion

4.1. Experimental verification of SPION assembly behaviors

The SPION assembly behaviors depicted in Section 3.1 were confirmed during real-time experimental observation. Upon application of a static magnetic field, needle-like anisotropic assemblies were formed (see Fig. 4a); zippering was observed after 5 min as the assembly sizes became large and highly anisotropic (see Fig. 4b). The threshold magnetic field of 13 G (for 0.04 vol% SPIONs in water) was also confirmed; free aggregates were left non-assembled with the 10 G field, while all aggregates formed assemblies with the 50 G field (see Fig. 4c). Below, magnetic assembly is conducted with a field stronger than 10 G so that quantitative evaluation of SPION assembly feature sizes can be fairly compared without the presences of free aggregates.

4.2. Tailoring of SPION assemblies in DI water with oscillating magnetic fields

The SPION assembly morphologies were captured (see Fig. 5) and measured (see Fig. 6) for each magnetic assembly condition to evaluate the theory of transverse assembly introduction using the oscillating magnetic field described in Section 3.2. A 95% bootstrap confidence interval based on the mean parameter values is indicated in the figures. As shown in Fig. 6, when the oscillation is turned on, the assemblies become longer, wider, and more separated, which can be attributed to introduction of the transverse assembly mechanism (see Fig. 2). Meanwhile, with a higher flux density, lateral assembly becomes dominant and therefore the assemblies become longer, thinner and less separated, except for the assemblies formed with the fields of the sinusoidal waveform and low frequency. As the frequency decreases, the assembly lengths and widths increase, regardless of the waveform type, but the assembly separation trends vary based on the waveform type. As the frequency decreases, the separations produced by the sinusoidal waveform increase, while the separations produced by the square waveform decrease. This discrepancy can be attributed to the SPION particle rotation behavior differences due to the waveform type (see Fig. 3a). With the gradual transition of the sinusoidal waveform, the SPIONs gradually rotate and thus have enough time to complete transverse assembly which also increases the separation between assemblies. Meanwhile, with the abrupt transition of the square waveform, the SPIONs rotate to briefly promote transverse assembly, but then quickly align their magnetic moment with the new field direction, and thus have more time to complete lateral assembly.

The effects of SPION volume fraction on their magnetic assembly were also studied (see Fig. 7). With higher SPION volume fractions, the distances between SPION aggregates are smaller; both lateral and transverse assemblies are enhanced resulting in increases to the assembly length and width. The SPION volume fraction was kept low in this study to enable in-situ assembly observation using optical microscopy. With higher SPION volume fractions, the assemblies are expected to span the entire sample domain.

One-dimensional tuning of SPION assemblies has been demonstrated through modulated introduction of transverse assembly using the oscillating magnetic fields. Compared with SPION assemblies achieved with the static field, the assembly morphology by the sinusoidal oscillating field exhibited changes by as much as 43% increase for the length (100 G, 0.1 Hz), 56% for the width (100 G, 0.05 Hz), and 139% for the separation (100 G, 0.05 and 0.1 Hz). Such line assembly patterning capability will be effective to tailor, for example, transport properties of PNCs: with the same nanofiller volume fraction, thin, long, and dense line features are more likely to extend across the sample size

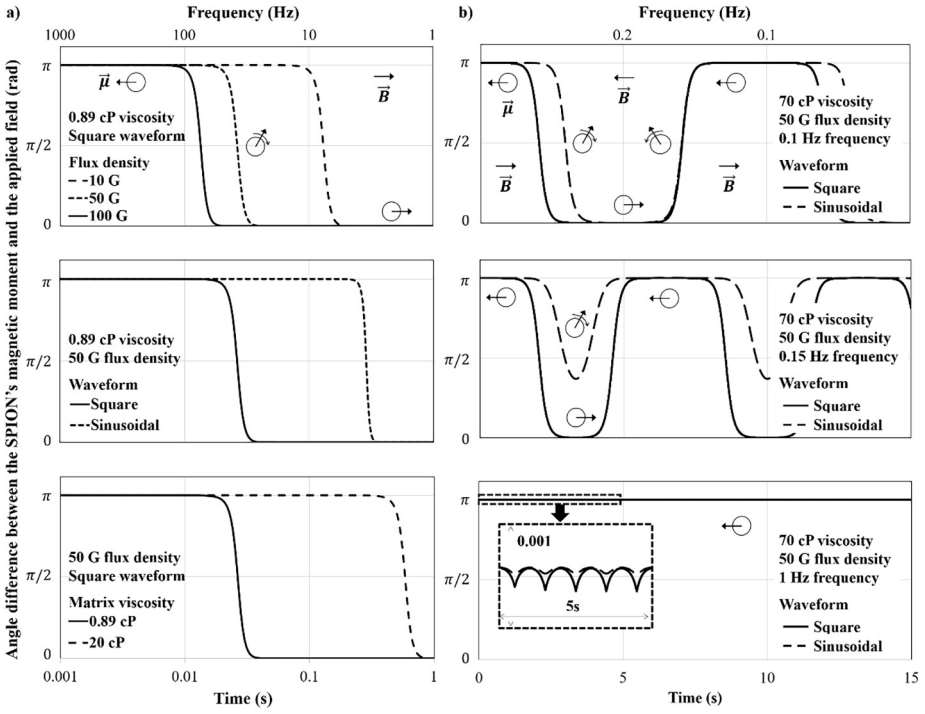

Fig. 3. Calculated Brownian rotation angle of a model spherical SPION over time in oscillating magnetic fields: a) magnetic moment rotation slowed down by smaller flux density (top), by sinusoidal waveform (middle), and by higher matrix viscosity (bottom), and b) slow magnetic moment rotation (top) or incomplete rotation (middle and bottom) with increasing field oscillation frequency.

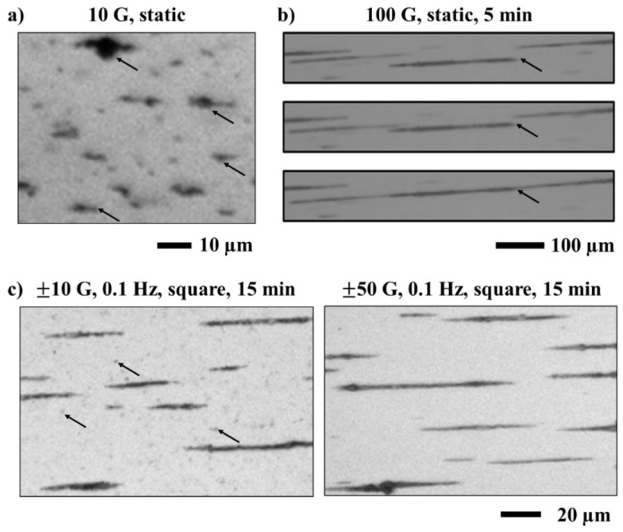

Fig. 4. Optical microscope images of SPION assembly in DI water (0.04 vol%): a) needle-like assemblies upon static field application, b) zippering, and c) free aggregates (left) vs. complete assembly (right) by varying the field flux density.

with minimum interfaces and thus boundaries resistance, resulting in higher transport properties.

4.3. Tunable magnetic assembly of ferrimagnetic iron oxide nanoparticles

Ferrimagnetic nanoparticles are more magnetically responsive than SPIONs, although with remanence. Thus, ferrimagnetic nanoparticles can provide stronger inter-particle magnetic forces to overcome hydrodynamic drag, and therefore are suitable for assembly in viscous polymers. First, magnetic assembly behaviors were studied about ferrimagnetic iron oxide nanoparticles (US Research Nanomaterials, US7568, Fe_3O_4, approximately 20 nm diameter, 1–5 μm aggregate size, 60 emu/g saturation) in DI water and were compared with those of the SPIONs (see Fig. 8) to evaluate the effect of nanoparticle's magnetic properties on assembly behaviors. With the static field application (50 G, 10 min), the Fe_3O_4 assembly length (139 μm) and separation (61 μm) were much larger than those of SPION assemblies (25 μm length and 18 μm separation) of the same volume fraction (0.04 vol%). With the stronger magnetic susceptibility of Fe_3O_4, the capture radius increases and thus head-to-tail assembly is promoted, resulting in longer assemblies with larger separation. An unexpected trend was observed when the field oscillation was turned on (0.05 Hz, 50 G, square waveform); the Fe_3O_4 assembly length decreased (45 μm), while the SPION assembly length always increased with the square field oscillation, especially in the low frequency range, as shown in the SPION assembly study in Section 4.2. It should be noted that this Fe_3O_4 assembly length (45 μm by the square waveform with 0.05 Hz and 50 G) is comparable with the SPION assembly length achieved with the similar oscillating field (37 μm by the square waveform with 0.1 Hz and 50 G). In addition, the Fe_3O_4 assembly separation (106 μm by the square waveform with 0.05 Hz and 50 G) is much larger than those of Fe_3O_4 assembly by the static field (61 μm by the static field of 50 G) and of the SPION assembly achieved with the similar oscillating field (23 μm by the square waveform with 0.1 Hz and 50 G). Assuming that magnetic moment reorientations can be completed with this low frequency field oscillation (0.05 Hz), this unexpected trend can be attributed to enhanced transverse assembly due to the larger magnetic susceptibility; free aggregates are effectively attracted to assemblies, leading to the separations between assemblies becoming larger than the capture radius, effectively prohibiting head-to-tail and/or zippering assembly. By increasing the field strength to 100 G, the Fe_3O_4 assembly length increased (121 μm by the square waveform with 0.05 Hz and 100 G) while keeping the separation relatively large (89 μm) because the capture radius was increased and thus the head-to-tail and/or zippering assembly were enabled. This assembly study confirmed that the magnetic properties of the nanofillers play a large role in assembly formation by inter-assembly attraction rather than by aggregate attraction to assemblies. This capability to lengthen assemblies is effective to achieve percolation within nanocomposites and thus higher transport properties. Further studies should be conducted to explore more tailorability of ferrimagnetic nanofiller assembly, for example to decrease the separation while maintaining assembly lengths.

Lastly, PNCs with varying 1D alignment patterns were fabricated

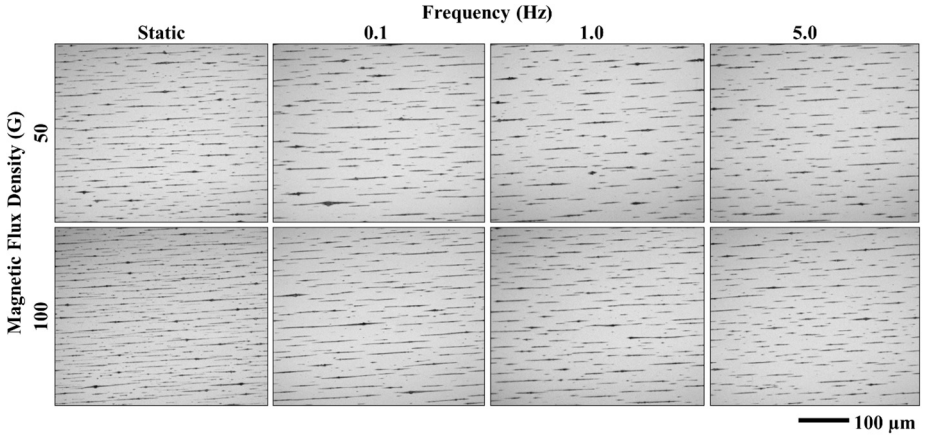

Fig. 5. Selected microscope images of SPION assemblies in DI water (0.04 vol%) using the square oscillating magnetic fields of varying magnetic flux density and frequency.

using another but similar ferrimagnetic iron oxide nanofillers (US Research Nanomaterials, US3200, γ-Fe_2O_3, approximately 25 nm diameter, 1–10 μm aggregate size, 57 emu/g saturation, 0.026 g) and EPON 862 (bisphenol-F thermoset, Hexion) resin with Epikure W curing agent (see Fig. 9). This epoxy was aerospace grade, commercially available, and with low viscosity. A 100:26.4 standard mass ratio of the resin-to-the-curing agent was used. Nanofiller-polymer mixtures (0.1 vol%) were prepared by ultrasonication (30 min at 60 °C) and were poured into a mold (3.18 cm × 3.18 cm × 0.508 cm). The mixture was heated to the working temperature of 70 °C; the mixture viscosity was measured as 70 cP at this temperature using a viscometer (Brookfield, RVTDV-IICP). A static magnetic field (50 G and 100 G) was applied

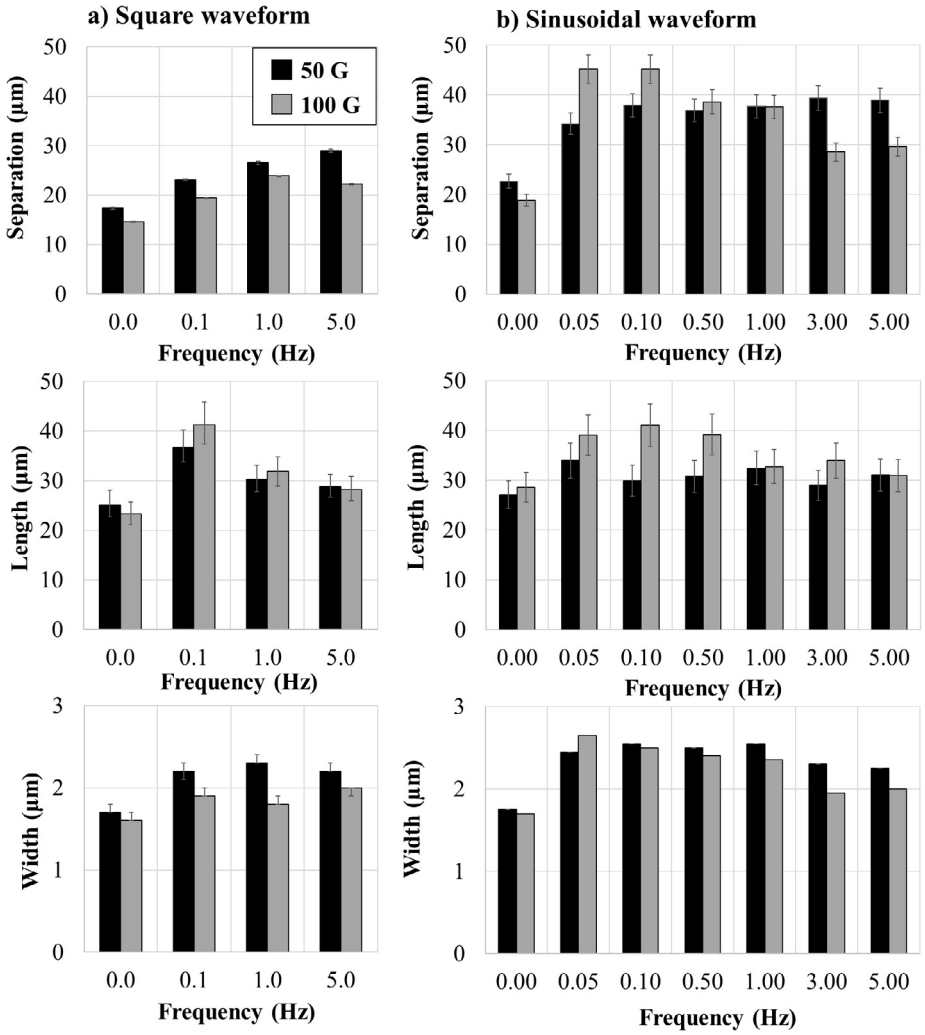

Fig. 6. Measured morphologies of SPION assemblies in DI water using oscillating magnetic fields of varying magnetic flux density, frequency, and waveform: a) 0.04 vol%, square waveform, and b) 0.02 vol%, sinusoidal waveform.

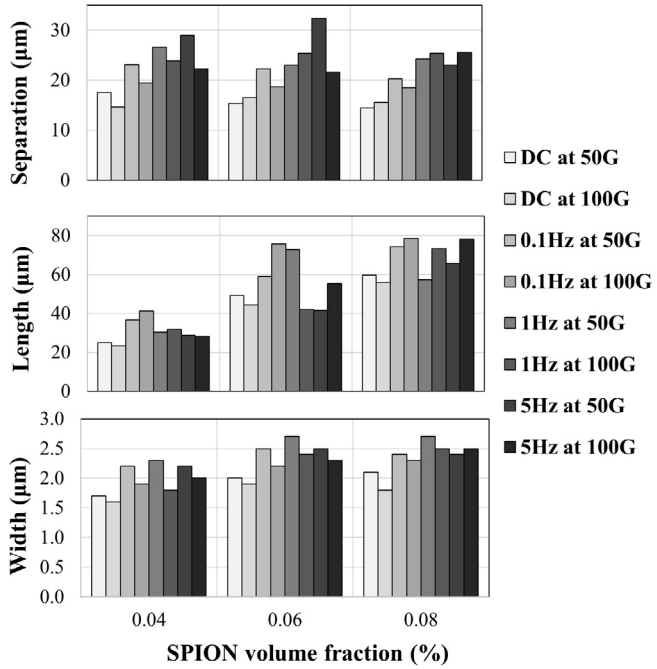

Fig. 7. Measured morphologies of SPION assemblies in DI water using oscillating magnetic fields with square waveform of varying SPION volume fractions.

across the mixture for 30 min at 70 °C, and then cured following the standard cycle: 121 °C for 1 h with the magnetic field applied and 171 °C for 2 h in an oven. As shown in Fig. 9, linear nanoparticle patterning was achieved using small magnetic fields (< 100 G) even in a viscous matrix with a assembly time of 30 min. Migration of the γ-Fe_2O_3 particles towards the poles was observed due to the large field gradient (> 10%) across the sample domain (3.18 cm length). In this viscous matrix, the assembled lines were observed to be thicker (compare Fig. 9b with Fig. 8b). This trend can be attributed to the higher nanofiller volume fraction, and also to the difficulty of nanoparticle dispersion within the matrix. The longer assembly time (30 min vs. 10–15 min in DI water) was also necessary so that the aggregates have enough time to assemble with the increased hydrodynamic forces. Nanoparticle patterning, including tuning of inter-nanoparticle contacts, was attained by varying the field flux density; dense thin lines were achieved with the 50 G field while sparse thick lines were observed with the 100 G field because the stronger field flux density enhanced head-to-tail attraction and zippering. In our next work, the fabricated PNCs will be inspected for their nanofiller structures using 3D tomography and characterized for their anisotropic transport properties. The structure-property relationships will be investigated, especially about the effect of interphases on transport properties.

5. Conclusion

Active assembly using external magnetic fields was studied as a scalable and energy-efficient method to structure nanofillers and tailor their inter-particle contacts within polymer matrices to deliver anisotropic, multi-functional PNCs. The capability to tune one-dimensional line assemblies was studied and achieved using magnetically-responsive nanofillers (SPIONs, Fe_3O_4, and γ-Fe_2O_3, 0.02–0.1 vol%) in matrices (0.89 cP and 70 cP) by applying oscillating magnetic fields of various frequencies (< 5 Hz), waveforms (sinusoidal vs. square), and field flux densities (< 100 G). The magnetic moment response to the oscillating magnetic fields used in this work is dominated by Brownian rotation, and their assembly mechanisms observed in this study are summarized below.

(1). With the static magnetic field, lateral assembly is dominant where free aggregates form assemblies along the field direction. The locally induced fields from such anisotropic assemblies enable head-to-tail assembly and zippering producing longer assemblies.
(2). When the field oscillation is turned on, and if the particles have enough time to respond with the changing fields (with low frequency and low matrix viscosity), transverse assembly will be introduced to promote more separated, wider, and longer assemblies.
(3). When the field oscillates, but if the particles do not have enough time to respond to the changing fields (with high frequency and high matrix viscosity), the particle magnetic moments will not rotate, and thus the assembly patterns will resemble those achieved by the static fields.
(4). When magnetic responsiveness of particles is strong, assembly morphologies generally increase due to enhanced inter-assembly attractions.

Our future work, based on the above obtained understanding, include two components. First, structure-property relationship studies, especially about the effects of the interphases, will be conducted by characterizing and comparing the fabricated PNCs of the same volume fractions but with different inter-nanofiller contacts: 3D distribution of

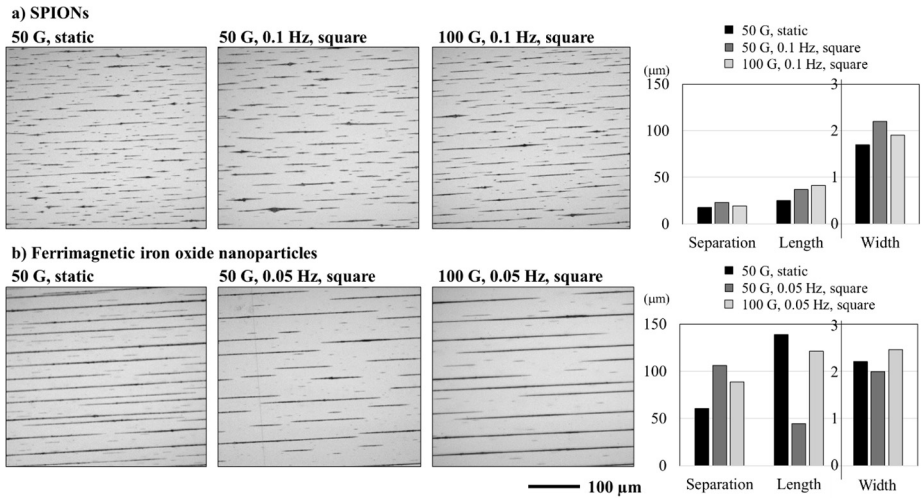

Fig. 8. Magnetic assembly comparison of a) SPIONs and b) ferrimagnetic Fe_3O_4 (both 0.04 vol% in DI water) by microscope images and measured assembly morphologies.

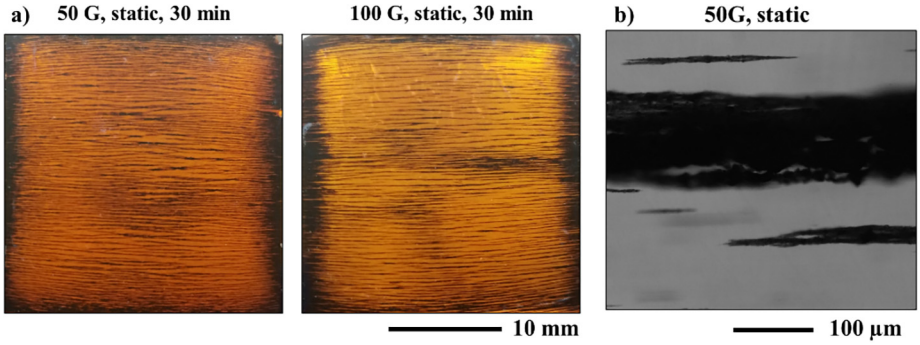

Fig. 9. Post cure digital images of 1D-patterned PNCs consisting of γ-Fe_2O_3 nanoparticles in a thermoset (0.1 vol%) using a static magnetic field of different flux densities: a) digital images, and b) microscope image.

nanofillers will be obtained using X-ray micro-CT scans, and anisotropic electrical and thermal conductivities will be measured. This study of PNCs with the small nanofiller volume fractions (< 0.1%) is relevant for thermal and electrical interface material application where effective percolation is expected with small nanofiller volume fraction and small boundary resistances [13,56]. Second, extended capability of magnetic structuring of PNCs will be tested for material systems consisting of various nanoparticles (magnetically responsive carbon nanotubes [57], surface treatment [30,58], higher volume fraction, etc.) and matrices (elastomers [59], UV-curable polymers, etc.) using triaxial Helmholtz coil set-up in our lab. Changes in magnetic assembly behaviors (tailorability, assembly time, and required field strength, etc.) will be evaluated, for example by stronger hydrodynamic forces with viscous polymers, enhanced nanofiller interactions with higher volume fraction, and changed nanofiller-polymer interactions with surface treatment.

Acknowledgements

This work was supported by the Office of Naval Research, Grant No. N00014161217, the Hartz Family Career Development Professorship in Engineering, and the Pennsylvania State University (PSU) Department of Aerospace Engineering. The authors would like to thank T. Clark and J. Gray from the Materials Characterization Lab at PSU for their assistance with TEM and SEM, Dr. Paris von Lockette and Corey Breznak for assistance with VSM measurements, Dr. Charles Bakis for supplying the first polymer samples, and Dr. Thomas Juska of the Applied Research Lab at PSU for assistance with fabrication of the polymer.

References

[1] H. Liu, L.C. Brinson, Reinforcing efficiency of nanoparticles: a simple comparison for polymer nanocomposites, Compos. Sci. Technol. 68 (2008) 1502–1512, https://doi.org/10.1016/j.compscitech.2007.10.033.
[2] I. Neitzel, V. Mochalin, I. Knoke, G.R. Palmese, Y. Gogotsi, Mechanical properties of epoxy composites with high contents of nanodiamond, Compos. Sci. Technol. 71 (2011) 710–716, https://doi.org/10.1016/j.compscitech.2011.01.016.
[3] S. Wu, R.B. Ladani, J. Zhang, A.J. Kinloch, Z. Zhao, J. Ma, X. Zhang, A.P. Mouritz, K. Ghorbani, C.H. Wang, Epoxy nanocomposites containing magnetite-carbon nanofibers aligned using a weak magnetic field, Polymer 68 (2015) 25–34, https://doi.org/10.1016/j.polymer.2015.04.080.
[4] M.A. Milani, D. Gonzalez, R. Quijada, N.R.S. Basso, M.L. Cerrada, D.S. Azambuja, G.B. Galland, Polypropylene/graphene nanosheet nanocomposites by in situ polymerization: synthesis, characterization and fundamental properties, Compos. Sci. Technol. 84 (2013) 1–7, https://doi.org/10.1016/j.compscitech.2013.05.001.
[5] Y.L. Liang, R.A. Pearson, Toughening mechanisms in epoxy-silica nanocomposites (ESNs), Polymer 50 (2009) 4895–4905, https://doi.org/10.1016/j.polymer.2009.08.014.
[6] P. Podsiadlo, A.K. Kaushik, E.M. Arruda, A.M. Waas, B.S. Shim, J. Xu, H. Nandivada, B.G. Pumplin, J. Lahann, A. Ramamoorthy, N. Kotov, Ultrastrong and stiff layered polymer nanocomposites, Science 318 (2007) 80–83, https://doi.org/10.1126/science.1143176.
[7] M.T. Byrne, Y.K. Gun'ko, Recent advances in research on carbon nanotube-polymer composites, Adv. Mater. 22 (2010) 1672–1688, https://doi.org/10.1002/adma.200901545.
[8] R.B. Ladani, S. Wu, A.J. Kinloch, K. Ghorbani, A.P. Mouritz, C.H. Wang, Enhancing fatigue resistance and damage characterisation in adhesively-bonded composite joints by carbon nanofibres, Compos. Sci. Technol. 149 (2017) 116–126, https://doi.org/10.1016/j.compscitech.2017.06.018.
[9] S. Wu, R.B. Ladani, A.R. Ravindran, J. Zhang, A.P. Mouritz, A.J. Kinloch, C.H. Wang, Aligning carbon nanofibres in glass-fibre/epoxy composites to improve interlaminar toughness and crack-detection capability, Compos. Sci. Technol. 152 (2017) 46–56, https://doi.org/10.1016/j.compscitech.2017.09.007.
[10] T. Kashiwagi, F. Du, J.F. Douglas, K.I. Winey, R.H. Harris, J.R. Shields, Nanoparticle networks reduce the flammability of polymer nanocomposites, Nat. Mater. 4 (2005) 928–933, https://doi.org/10.1038/nmat1502.
[11] G.R. Ruschau, S. Yoshikawa, R.E. Newnham, Resistivities of conductive composites, J. Appl. Phys. 72 (1992) 953–959, https://doi.org/10.1063/1.352350.
[12] A.I. Oliva-Avilés, F. Avilés, V. Sosa, Electrical and piezoresistive properties of multi-walled carbon nanotube/polymer composite films aligned by an electric field, Carbon 49 (2011) 2989–2997, https://doi.org/10.1016/j.carbon.2011.03.017.
[13] A.A. Novakova, V.Y. Lanchinskaya, A.V. Volkov, T.S. Gendler, T.Y. Kiseleva, M.A. Moskvina, S.B. Zezin, Magnetic properties of polymer nanocomposites containing iron oxide nanoparticles, J. Magn. Magn. Mater. 258–259 (2003), https://doi.org/10.1016/S0304-8853(02)01062-4.
[14] H. Wang, G. Wang, W. Li, Q. Wang, W. Wei, Z. Jiang, S. Zhang, A material with high electromagnetic radiation shielding effectiveness fabricated using multi-walled carbon nanotubes wrapped with poly(ether sulfone) in a poly(ether ether ketone) matrix, J. Mater. Chem. 22 (2012) 21232, https://doi.org/10.1039/c2jm35129c.
[15] S.V. Ahir, E.M. Terentjev, Photomechanical actuation in polymer-nanotube composites, Nat. Mater. 4 (2005) 491–495, https://doi.org/10.1038/nmat1391.
[16] F. Fahrni, M.W.J. Prins, L.J. van IJzendoorn, Magnetization and actuation of polymeric microstructures with magnetic nanoparticles for application in microfluidics, J. Magn. Magn. Mater. 321 (2009) 1843–1850, https://doi.org/10.1016/j.jmmm.2008.11.090.
[17] J.M. Wernik, S.A. Meguid, Recent developments in multifunctional nanocomposites using carbon nanotubes, Appl. Mech. Rev. 63 (2010) 050801, , https://doi.org/10.1115/1.4003503.
[18] R.R. Mitchell, N. Yamamoto, H. Cebeci, B.L. Wardle, C.V. Thompson, A technique for spatially-resolved contact resistance-free electrical conductivity measurements of aligned-carbon nanotube/polymer nanocomposites, Compos. Sci. Technol. 74 (2013) 205–210, https://doi.org/10.1016/j.compscitech.2012.11.003.
[19] A.M. Marconnet, N. Yamamoto, M.A. Panzer, B.L. Wardle, K.E. Goodson, Thermal conduction in aligned carbon nanotube-polymer nanocomposites with high packing density, ACS Nano 5 (2011) 4818–4825, https://doi.org/10.1021/nn200847u.
[20] R.M. Erb, R. Libanori, N. Rothfuchs, A.R. Studart, Composites reinforced in three dimensions by using low magnetic fields, Science 335 (2012) 199–204.
[21] C.B. Murray, C.R. Kagan, M.G. Bawendi, Synthesis and characterization of monodisperse nanocrystals and close-packed nanocrystal assemblies, Annu. Rev. Mater. Sci. 30 (2000) 545–610.
[22] V.P. Veedu, A. Cao, X. Li, K. Ma, C. Soldano, S. Kar, P.M. Ajayan, M.N. Ghasemi-Nejhad, Multifunctional composites using reinforced laminae with carbon-nanotube forests, Nat. Mater. 5 (2006) 457–462, https://doi.org/10.1038/nmat1650.
[23] E.J. Garcia, B.L. Wardle, A. John Hart, N. Yamamoto, Fabrication and multifunctional properties of a hybrid laminate with aligned carbon nanotubes grown in situ, Compos. Sci. Technol. 68 (2008) 2034–2041, https://doi.org/10.1016/j.compscitech.2008.02.028.
[24] J. Park, K.H. Lee, Carbon nanotube yarns, Korean J. Chem. Eng. 29 (2012) 277–287, https://doi.org/10.1007/s11814-012-0016-1.
[25] Y. Liu, H. Lv, X. Lan, J. Leng, S. Du, Review of electro-active shape-memory polymer composite, Compos. Sci. Technol. 69 (2009) 2064–2068, https://doi.org/10.1016/j.compscitech.2008.08.016.
[26] A.I. Oliva-Avilés, F. Avilés, V. Sosa, A.I. Oliva, F. Gamboa, Dynamics of carbon nanotube alignment by electric fields, Nanotechnology 23 (2012), https://doi.org/10.1088/0957-4484/23/46/465710.
[27] J. Shi, D. Ahmed, X. Mao, S.C. Lin, A. Lawit, T.J. Huang, Acoustic tweezers: patterning cells and microparticles using standing surface acoustic waves (SSAW), Lab Chip 9 (2009) 2890–2895, https://doi.org/10.1039/b910595f.
[28] R.A. Vaia, J.F. Maguire, Polymer nanocomposites with prescribed morphology: going beyond nanoparticle-filled polymers, Chem. Mater. 19 (2007) 2736–2751,

https://doi.org/10.1021/cm062693+.
[29] R. Libanori, R.M. Erb, A.R. Studart, Mechanics of platelet-reinforced composites assembled using mechanical and magnetic stimuli, ACS Appl. Mater. Interfaces 5 (2013) 10794–10805, https://doi.org/10.1021/am402975a.
[30] M.Z. Rong, M.Q. Zhang, W.H. Ruan, Surface modification of nanoscale fillers for improving properties of polymer nanocomposites: a review, Mater. Sci. Technol. 22 (2006) 787–796, https://doi.org/10.1179/174328406X101247.
[31] D. Wirtz, M. Fermigier, One-Dimensional Patterns and Wavelength Selection in Magnetic Fluids, Phys. Rev. Lett. 72 (1994) 2294–2297.
[32] R.M. Erb, J. Segmehl, M. Charilaou, J.F. Löffler, A.R. Studart, Non-linear alignment dynamics in suspensions of platelets under rotating magnetic fields, Soft Matter. 8 (2012) 7604–7609, https://doi.org/10.1039/c2sm25650a.
[33] H. Garmestani, M.S. Al-Haik, K. Dahmen, R. Tannenbaum, D. Li, S.S. Sablin, M. Yousuff, Hussaini, Polymer-mediated alignment of carbon nanotubes under high magnetic fields, Adv. Mater. 15 (2003) 1918–1921, https://doi.org/10.1002/adma.200304932.
[34] P.A. Valberg, J.P. Butler, Magnetic particle motions within living cells – physical theory and techniques, J. Biol. Soc. 52 (1987) 537–550, https://doi.org/10.1016/S0006-3495(87)83243-5.
[35] A. Jordan, R. Scholz, P. Wust, H. Fähling, R. Felix, Magnetic fluid hyperthermia (MFH): cancer treatment with AC magnetic field induced excitation of biocompatible superparamagnetic nanoparticles, J. Magn. Magn. Mater. 201 (1999) 413–419, https://doi.org/10.1016/S0304-8853(99)00088-8.
[36] B.B. Yellen, R.M. Erb, H.S. Son, R. Hewlin Jr., H. Shang, G.U. Lee, Traveling wave magnetophoresis for high resolution chip based separations, Lab Chip 7 (2007) 1681–1688, https://doi.org/10.1039/B713547E.
[37] S. Miltenyi, W. Müller, W. Weichel, A. Radbruch, High gradient magnetic cell separation with MACS, Cytometry 11 (1990) 231–238, https://doi.org/10.1002/cyto.990110203.
[38] J.W. Swan, J.L. Bauer, Y. Liu, E.M. Furst, Directed colloidal self-assembly in toggled magnetic fields, Soft Matter. 10 (2014) 1102–1109, https://doi.org/10.1039/c3sm52663a.
[39] T. Allen, Particle Size Measurement, first ed., Chapman & Hall, London, 1968.
[40] J.-S.D. Schnyder, Magnetic characterization of iron oxide nanoparticles, ETH Zürich (2010).
[41] D. Pouliquen, H. Perroud, F. Calza, P. Jallet, J.J. Le Jeune, Investigation of the magnetic properties of iron oxide nanoparticles used as contrast agent for MRI, Magn. Reson. Med. 24 (1992) 75–84, https://doi.org/10.1002/mrm.1910240108.
[42] M.P. Spencer, N. Yamamoto, Nanoparticle Alignment using Oscillating Magnetic Fields for Scalable Nanocomposite Manufacturing, in: 57th AIAA/ASCE/AHS/ASC Struct. Struct. Dyn. Mater. Conf. San Diego, California, USA, 2016. doi:10.2514/6.2016-0150.
[43] Q. Li, C.W. Kartikowati, S. Horie, T. Ogi, T. Iwaki, K. Okuyama, Correlation between particle size/domain structure and magnetic properties of highly crystalline Fe3O4 nanoparticles, Sci. Rep. 7 (2017) 9894, https://doi.org/10.1038/s41598-017-09897-5.
[44] V. Schaller, U. Kraling, C. Rusu, K. Petersson, J. Wipenmyr, A. Krozer, G. Wahnstrom, A. Sanz-Velasco, P. Enoksson, C. Johansson, Motion of nanometer sized magnetic particles in a magnetic field gradient, J. Appl. Phys. 104 (2008) 093918Artn 093918\n 10.1063/1.3009686.
[45] R.A. Ortega, T.D. Giorgio, A mathematical model of superparamagnetic iron oxide nanoparticle magnetic behavior to guide the design of novel nanomaterials, J. Nanoparticle Res. 14 (2012), https://doi.org/10.1007/s11051-012-1282-x.
[46] R. Dhavalikar, L. Maldonado-Camargo, N. Garraud, C. Rinaldi, Ferrohydrodynamic modeling of magnetic nanoparticle harmonic spectra for magnetic particle imaging, J. Appl. Phys. 118 (2015) 173906, , https://doi.org/10.1063/1.4935158.
[47] B. Bharti, A.L. Fameau, O.D. Velev, Magnetophoretic assembly of flexible nanoparticles/lipid microfilaments, Faraday Discuss. 181 (2015) 437–448, https://doi.org/10.1039/c4fd00272e.
[48] N.S.S. Mousavi, S.D. Khapli, S. Kumar, Direct observations of field-induced assemblies in magnetite ferrofluids, J. Appl. Phys. 117 (2015) 1–9, https://doi.org/10.1063/1.4914484.
[49] A.E. Deatsch, B.A. Evans, Heating efficiency in magnetic nanoparticle hyperthermia, J. Magn. Magn. Mater. 354 (2014) 163–172, https://doi.org/10.1016/j.jmmm.2013.11.006.
[50] S. Van Berkum, J.T. Dee, A.P. Philipse, B.H. Ern, Frequency-dependent magnetic susceptibility of magnetite and cobalt ferrite nanoparticles embedded in PAA hydrogel, Int. J. Mol. Sci. 14 (2013) 10162–10177, https://doi.org/10.3390/ijms140510162.
[51] P. De La Presa, Y. Luengo, M. Multigner, R. Costo, M.P. Morales, G. Rivero, A. Hernando, Study of heating efficiency as a function of concentration, size, and applied field in gamma-Fe2O3 nanoparticles, J. Phys. Chem. C 116 (2012) 25602–25610, https://doi.org/10.1021/jp310771p.
[52] B. Jeyadevan, Present status and prospects of magnetite nanoparticles-based hyperthermia, J. Ceram. Soc. Jpn. 118 (2010) 391–401, https://doi.org/10.2109/jcersj2.118.391.
[53] C.S.S.R. Kumar, Magnetic Characterization Techniques for Nanomaterials, 2017, doi:10.1007/978-3-662-52780-1.
[54] J. Leliaert, A. Coene, G. Crevecoeur, A. Vansteenkiste, D. Eberbeck, F. Wiekhorst, U. Steinhoff, B. Van Waeyenberge, L. Dupr, Regarding the Neel relaxation time constant in magnetorelaxometry, J. App. Phys. 116 (2014) 1–4, https://doi.org/10.1063/1.4900916.
[55] S.H. Lamb, Hydrodynamics, sixth ed., Dover Publications, New York, 1945.
[56] J.L. Wilson, P. Poddar, N.A. Frey, H. Srikanth, K. Mohomed, J.P. Harmon, S. Kotha, J. Wachsmuth, Synthesis and magnetic properties of polymer nanocomposites with embedded iron nanoparticles, J. Appl. Phys. 95 (2004) 1439–1443, https://doi.org/10.1063/1.1637705.
[57] J. Haibat, S. Ceneviva, M.P. Spencer, F. Kwok, S. Trivedi, S.E. Mohney, N. Yamamoto, Preliminary demonstration of energy-efficient fabrication of aligned CNT-polymer nanocomposites using magnetic fields, Compos. Sci. Technol. 152 (2017) 27–35, https://doi.org/10.1016/j.compscitech.2017.09.006.
[58] J. Gass, P. Poddar, J. Almand, S. Srinath, H. Srikanth, Superparamagnetic polymer nanocomposites with uniform Fe3O4 nanoparticle dispersions, Adv. Funct. Mater. 16 (2006) 71–75, https://doi.org/10.1002/adfm.200500335.
[59] Y. Atescan, M.P. Spencer, N. Yamamoto, Triaxial Magnetic Assembly of Polymer Nanocomposites, in: 60th AIAA/ASCE/AHS/ASC Struct. Struct. Dyn. Mater. Conf., San Diego, CA, 2019.